ACS OMEGA

Open Access

http://pubs.acs.org/journal/acsodf

Article

Optimization of Flow Channels in a PEM Fuel Cell Based on a Multiobjective Evaluation

Dong Jiang, Fangzhou Wang,* Xianglin Li, Jianyu Tan,* and Chenxia Wang

Cite This: *ACS Omega* 2024, 9, 1683−1694

Read Online

ACCESS | Metrics & More | Article Recommendations | Supporting Information

ABSTRACT: Proton exchange membrane fuel cells (PEMFCs) are known for their cleanliness and high efficiency. However, the limited energy density and high cost are the main obstacles to this technology. This study aims to overcome these challenges and enhance the overall performance of the PEMFC. Five types of PEMFCs with different blockages are proposed and simulated in this study. Afterward, the Technique for Order Preference by Similarity to Ideal Solution (TOPSIS) method is performed as a multiobjective evaluation. This study shows that the nozzle effect in the channel enhances the mass transfer of PEMFC and improves water and thermal management, resulting in a reduction of liquid water by up to 35.8%. The blockages benefit the output performance of the PEMFC. For example, the elliptical blockage shows the highest improvement in electrochemical conversion efficiency at 3.42%. The TOPSIS examines indices of power, exergy, economy, environment, and water and thermal management. The multiobjective evaluation shows that the elliptical blockage is more beneficial for PEMFC. This study provides an optimized design of the PEMFC flow channel and a new perspective to evaluate the structural improvement of PEMFC.

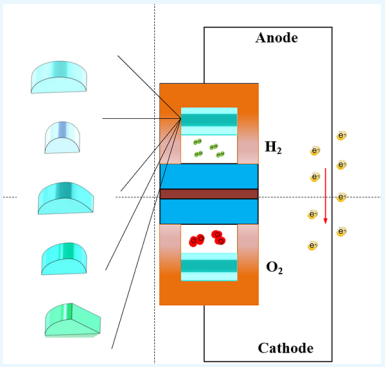

1. INTRODUCTION

Energy storage technology, including Lithium-ion batteries[1,2] and emerging hydrogen-based systems, is pivotal for the energy sector, offering high energy density and emissions-free advantage. Fuel cell is a vital technology for utilizing hydrogen energy due to its high efficiency and low or zero emissions.[3−5] The main types of fuel cells currently include proton exchange membrane fuel cell (PEMFC), alkaline fuel cell (AFC), phosphoric acid fuel cell (PAFC), solid oxide fuel cell (SOFC), and molten carbonate fuel cell (MCFC).[6−8] Among these, PEMFC has the advantages of being clean, having a low working temperature, and having a low noise. Therefore, it is widely applied in transportation and housing.[9]

Several factors influence the performance of PEMFCs, including electrochemical reaction rates, heat transfer, and drainage.[10−15] Currently, water and thermal management are the main focus for improving the output performance of PEMFCs.[16,17] Maintaining optimal levels of humidity within the membrane is crucial to achieving high proton conductivity, which is directly related to water content.[18] However, excessive moisture can lead to blockages in flow channels and gas diffusion layer pores, resulting in reactant starvation.[19] On the other hand, effective thermal management is also essential for maintaining high stability in PEMFC. High temperatures can cause dehydration of the proton exchange membrane and decrease conductivity, while low temperatures can impede reaction rates and ion transmission[20] Additionally, uniform temperature distribution across the cell is important. In the operation of the PEMFC, effective strategies of water and thermal management are highly required.

The structure of flow channels plays a crucial role in managing water, thermal energy, and mass transfer in PEMFCs.[21] A well-designed flow field structure can facilitate mass transfer between channels and gas diffusion layers, optimize water and thermal management, and increase power density. Li et al.[22] studied a wavy surface in the cathode channel and found that the design improved oxygen transport and reduced water saturation. Perng and Wu[23] investigated PEMFC with trapezoidal baffles. When compared to the traditional unbaffled flow channel, a new trapezoidal baffle design (a 60° angle and a 1.125 mm height) has resulted in a notably higher net power output of the fuel cell. Specifically, among the various trapezoidal baffle designs, this particular configuration achieved an impressive 90% increase in net power. Shen et al.[24] applied the field synergy principle to analyzing PEMFC with four different blockages in the flow channel. The findings showed that the blockage blocks led to an increase in the effective mass transfer coefficient and hence the energy performance of the PEMFC. Zhang et al.[25] put forward a single-channel PEMFC with wedge-shaped fins in the cathode channel. They studied the effect of the wedge-shaped fin shape on the polarization curve and power density curve. The results showed that the oxygen mass fraction distribution in the exit

Received: October 21, 2023
Revised: November 30, 2023
Accepted: December 5, 2023
Published: December 22, 2023

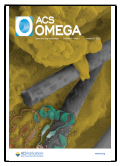

region of the cathode channel was smaller as the fin volume increased. Meanwhile, the drainage effect of PEMFC was improved, and the growth rate of power density was enhanced accordingly. Li et al.[26] proposed a bionic flow channel design inspired by the internal structure of the nautilus. The research results demonstrate that the Nautilus bionic flow channel outperforms the other two designs in terms of reactant distribution, water removal efficiency, concentration polarization loss reduction, and enhanced power generation performance. Compared with the serpentine flow channel, the Nautilus design exhibits a 46.7% increase in peak current density and a 21.53% increase in peak power density. In comparison to the honeycomb flow channel, the Nautilus design shows a 5.73% increase in the peak current density, while the power density remains similar. Therefore, the Nautilus bionic flow channel surpasses the honeycomb flow channel in terms of reactant uniformity, current density, and moisture removal capacity. Gao et al.[27] designed a novel foam-rib composite flow field structure, integrating the advantages of both metal foam flow field and traditional rib flow field. The experimental results demonstrate that the foam-rib composite flow field achieves a higher peak power density and ultimate current density compared to the traditional rib flow field. Specifically, when the optimal metal foam filling ratio is 0.75 and the porosity is 0.85, the foam-rib composite flow field exhibits a 5.20% increase in the peak power density and a 22.68% increase in the ultimate current density. Xia et al.[28] developed a new flow field structure for PEMFCs inspired by leaf veins and birds. The design included water droplets and flow blocks modeled after birds, which were incorporated into the branching channels of the structure. Simulation results indicated that this new composite bionic flow field promoted the uniform distribution of reaction gases and current density, thus improving the energy performance and the long-term stability of PEMFCs.

As mentioned above, the optimization of the flow field structure has a positive effect on the removal of liquid water, temperature control, and reaction gas distribution. However, the introduction of a complex flow field structure increases the inlet and outlet pressure drop. Further, the parasitic power will increase. Consequently, streamlined structures were put forward and investigated. Guo et al.[30] proposed a new blockage structure based on the rectangular baffle and trapezoidal baffle. This structure can reduce the pumping power loss during reactant delivery while maintaining a high degree of gas perturbation, thus increasing the net power of the cell. Li et al.[29] initially utilized four distinct shapes of simulated water-drop blocks for designing the flow channel in PEMFC. They identified the most optimal block shape using numerical simulation analysis. Previous research has shown that streamlined structures are effective in the design of a PEMFC. However, the application of this approach in PEMFC design is limited, and a deeper understanding of its mechanism is needed. This study aims to clarify the understanding of streamlined design in PEMFC by investigating and evaluating this approach in more detail.

The optimization of the PEMFC design relies on specific objectives such as increasing power density, enhancing efficiency, or minimizing environmental impact. However, these objectives may not always be the most cost-effective option. Moreover, emphasizing economic considerations may also result in negative environmental consequences. Therefore, it is essential to adopt a comprehensive approach that evaluates various indicators of fuel cell performance to ensure that all aspects are considered. Barbir and Gomez[31] considered both performance and economy to determine the best efficiency of fuel cells for producing cost-effective electricity. The study found that the efficiency of fuel cells is not only dependent on their performance characteristics but also on their economy. The results demonstrated that in the best-case scenario, the fuel cells can be produced at $100/kW, operate at 50% efficiency, and generate electricity at < $0.08/kWh if hydrogen can be supplied at $10/GJ. Taner[32] examined the performance of PEMFCs utilizing an open cathode plate configuration. They analyzed the effect of the operational pressure and voltage parameters on the PEMFC performance. Their findings indicated energy and exergy efficiencies of 47.6 and 50.4%, respectively. Bing et al.[33] conducted a comprehensive analysis of energy, exergy, environmental impact, and economic aspects of PEMFC using four dimensions. They thoroughly examined the performance indicators of various aspects of PEMFC and optimized them by using algorithms. It suggested that the performance metrics of PEMFC are diverse, including efficiency, energy, and other aspects. The common method for the comprehensive analysis of multiple indicators is the composite evaluation method. Composite evaluation methods include the Analytic Hierarchy Process (AHP), Entropy Weight Method, and the Technique for Order Preference by Similarity to Ideal Solution (TOPSIS).[34,35] However, these methods are rarely applied to PEMFC analysis. Hou et al.[36] provided an AHP-based evaluation method, proposing some basic performance metrics to evaluate the overall performance and giving arithmetic examples. However, the subjective nature of AHP renders the weighted values of the indicators to be unproven and unconvincing. Additionally, the two-by-two comparison process of AHP makes it impractical to evaluate objects with multiple index values. Shanian[37] employed the TOPSIS method for the selection of metal bipolar plate materials. The method was used to assess each material choice based on specific criteria and provide practical application reference points. In PEMFC optimization designs, comprehensive evaluation algorithms are not commonly utilized, especially when it comes to comparative single-cell optimization solutions. The TOPSIS is a well-known multicriteria decision analysis (MCDA) method that can assist decision-makers in selecting the optimal solution from a limited number of options. Compared with other comprehensive evaluation methods, TOPSIS has several benefits. First, it accurately considers the raw data information, thereby reflecting the differences among evaluation solutions with precision. Second, TOPSIS is an objective evaluation method that can prevent errors that arise from subjective weights. Third, the TOPSIS method can handle indicators with different units and scales, making it insensitive to the scale of indicator data. Additionally, it provides scores for each solution by comparing the distance between each solution and the ideal solution as well as the negative ideal solution. TOPSIS is suitable for analyzing and evaluating multiple metrics for fuel cells since the results are more direct and understandable. In this study, the TOPSIS method will be first introduced for the evaluation of flow channel optimization cases.

This study applies a streamlined design approach to the flow channel of the PEMFC by proposing five different blockage shapes. The performance of PEMFC is evaluated through the simulation of polarization curves, power density curves, water, and thermal states. Multidimensional analysis is conducted to extract subindexes that assess various factors, including energy, exergy, environment, and economy. The optimal design case of the streamlined block is determined by TOPSIS. This study

https://doi.org/10.1021/acsomega.3c08298
ACS Omega 2024, 9, 1683−1694

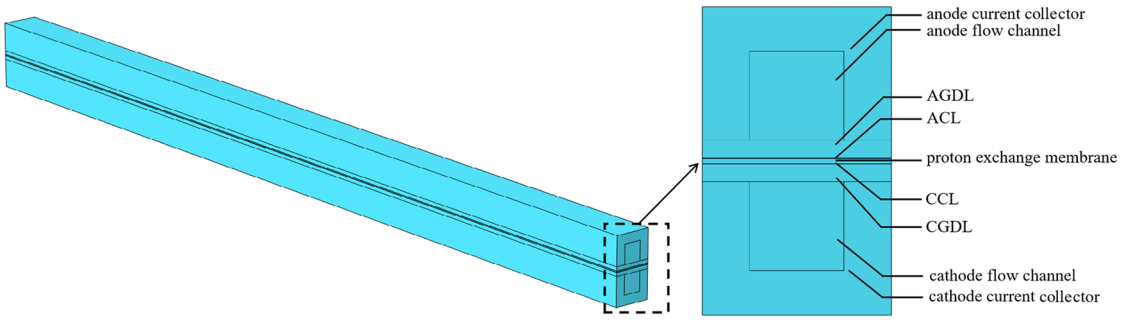

Figure 1. Structure of PEMFC.

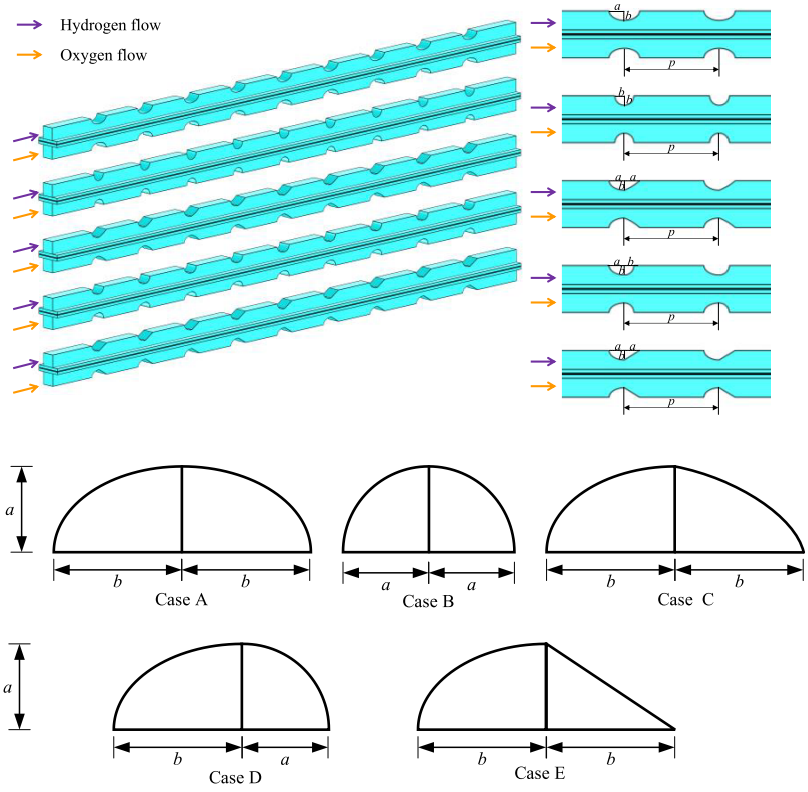

Figure 2. Sketch of five channels with the various shapes of the baffle.

presents a novel approach to PEMFC flow channel design and provides a multiobjective evaluation method for optimizing PEMFC cases.

2. PEMFC SIMULATION MODEL

2.1. Geometric Model. The PEMFC consists of nine parts: cathode/anode current collector, cathode/anode flow channel, cathode/anode gas diffusion layer (CGDL and AGDL), cathode/anode catalyst (CCL and ACL), and proton exchange membrane (PEM). The structure of the PEMFC is shown in Figure 1.

2.2. Computational Domain. The study investigates the effects of adding five streamlined blocking blocks of different shapes to the flow channel of a traditional flat channel PEMFC. The traditional channel is used as the reference model. The PEMFC flow channel without current collectors is shown in a 3D calculation domain in Figure 2. The blocking sections of Cases A and B are semiellipse and semicircle, respectively. Case C's blocking section consists of a quarter ellipse arc and a parabola. Case D's blocking section is composed of a quarter ellipse and a quarter circle arc, while Case E's blocking section is a Kax curve made up of a quarter ellipse arc and a straight line. Table 1 shows the parameters of the computed domain.

2.3. Governing Equations. The governing equations for PEMFC simulation calculation mainly include mass, momen-

Table 1. Geometric Parameters

	parameters	value	unit
length	L	50	mm
height of current collector	H_{cc}	1.5	mm
height of flow channel	H_{ch}	1	mm
thickness of membrane	H_{m}	0.05	mm
thickness of GDL	H_{gd}	0.2	mm
thickness of CL	H_{cl}	0.01	mm
width of the computational domain	W_{cd}	2	mm
width of the flow channel	W_{ch}	1	mm
length of block	a	0.8	mm
height of block	b	0.5	mm
interval of blocks	p	5	mm

https://doi.org/10.1021/acsomega.3c08298
ACS Omega 2024, 9, 1683−1694

tum, and energy conservation equations, electrochemical reaction equations, flow and mass transfer equations in porous media, and equations for the formation and transport of liquid water. The simulation model is solved using OpenFOAM and the operating conditions are presented in Table 2. The fundamental equations are listed below.

Table 2. Physical Parameters and Operating Conditions

parameters (unit)	value
equivalent weight of PEM (kg mol^{-1})[29]	2000
porosity (GDL, CL)[29]	0.4,0.5
transfer coefficients[29]	anode:0.5; cathode:0.5
contact angle (GDL, CL)(°)[29]	120, 100
permeability (m^2)[29]	$1e^{-12}$
electrical conductivity (current collector, GDL, CL) (S m^{-1})[29]	20,000, 5000, 2000
thermal conductivity (current collector, GDL, CL) (W m^{-1} K^{-1})[29]	20, 1, 0.95
reference hydrogen, oxygen concentrations (mol m^{-3})[29]	$C_{H_2}^{ref}$ = 56.4, $C_{O_2}^{ref}$ =3.39
anode reference exchange current density (A m^{-3})[29]	10^8
cathode reference exchange current density (A m^{-3})[29]	120
stoichiometry ratio[29]	anode:1.2; cathode:1.8
cell temperature (K)[29]	343.15
air relative humidity[29]	100%
H_2 relative humidity[29]	100%
open circuit voltage (V)[33]	0.95
standard chemical exergy of hydrogen (kJ $kmol^{-1}$)[33]	238,490
standard chemical exergy of oxygen (kJ $kmol^{-1}$)[33]	3970
standard chemical exergy of nitrogen (kJ $kmol^{-1}$)[33]	720
standard chemical exergy of water (kJ $kmol^{-1}$)[33]	3120

2.3.1. Mass Conversation.

$$\frac{\partial(\varepsilon\rho)}{\partial t} + \nabla(\varepsilon\rho\vec{u}) = S_m \tag{1}$$

where ρ is the density of the mixed gas and ε is porosity. For the flow channel, $\varepsilon = 1$; for the GDLs, $\varepsilon < 1$. S_m is the mass source term.

2.3.2. Momentum Conservation Equation.

$$\frac{\partial(\varepsilon\rho\vec{u})}{\partial t} + \nabla(\varepsilon\rho\vec{u}\vec{u}) = -\varepsilon\nabla p + \nabla(\varepsilon\mu\nabla\vec{u}) + S_u \tag{2}$$

where p is pressure, μ is the viscosity of the mixed fluid, and S_u is the source of momentum conservation.

2.3.3. Energy Conservation Equation.

$$\frac{\partial(\varepsilon\rho c_p T)}{\partial t} + \nabla(\varepsilon\rho c_p\vec{u}T) = \nabla\cdot(k^{eff}\nabla T) + S_Q \tag{3}$$

where k^{eff} is the effective thermal conductivity, T is the temperature, and c_p is constant pressure-specific heat capacity. S_Q is the energy source term.

2.3.4. Species Conservation Equation.

$$\frac{\partial(\varepsilon c_k)}{\partial t} + \nabla(\varepsilon\vec{u}c_k) = \nabla(D_k^{eff}\nabla c_k) + S_k \tag{4}$$

where c_k is the species concentration, D_k^{eff} is the species' effective diffusion coefficient. S_k denotes the species source term, and the subscript k denotes the component code. For the flow channel and diffusion layer, $S_k = 0$.

2.3.5. Conservation of Charge.

$$\nabla(\sigma_m\nabla\phi_m) + R_m = 0 \tag{5}$$

$$\nabla(\sigma_s\nabla\phi_s) + R_s = 0 \tag{6}$$

where σ_m and σ_s are electrical conductivity, ϕ_m and ϕ_s are the solid phase potential and the membrane phase potential. R_m and R_s are electron current sources and proton current source, respectively. In the anode, $R_s = -R_{an}$, $R_m = +R_{an}$; in the cathode, $R_s = +R_{cat}$, $R_m = -R_{cat}$.

$$R_{an} = R_{an}^{ref}\left(\frac{C_{H_2}}{C_{H_2}^{ref}}\right)^{\gamma_{an}}\left[\exp\left(\frac{\alpha_{an,an}F\eta_{an}}{RT}\right) - \exp\left(-\frac{\alpha_{cat,an}F\eta_{an}}{RT}\right)\right] \tag{7}$$

$$R_{cat} = R_{cat}^{ref}\left(\frac{C_{O_2}}{C_{O_2}^{ref}}\right)^{\gamma_{cat}}\left[\exp\left(\frac{\alpha_{cat,an}F\eta_{cat}}{RT}\right) - \exp\left(-\frac{\alpha_{an,cat}F\eta_{cat}}{RT}\right)\right] \tag{8}$$

where R_{an}^{ref} and R_{cat}^{ref} are the reference current densities, γ_{an} and γ_{cat} are concentration dependence, α is the transfer coefficient, and η is the local surface overpotential.

2.3.6. Gas Diffusion Equation.

$$q_y^k = -D_k\frac{\partial c_k}{\partial y} \tag{9}$$

where D_k is the diffusion coefficient of component k in porous media, and q_y^k is the diffusion flux of component k in the y-direction. Neglecting convective acceleration and diffusion, the laminar flow model in porous media degenerates to Darcy's law.

$$\nabla p = -\frac{\mu}{K}\vec{u} \tag{10}$$

2.3.7. Liquid Water Transport Equation. For gas channels,

$$\frac{\partial(\varepsilon\rho_l s)}{\partial t} + \nabla(s\rho_l\vec{u_l}) = r_w \tag{11}$$

$$r_w = c_r\max\left[(1-s)\frac{p_{ww} - p_{st}}{RT}M_{H_2O}, -s\rho_l\right] \tag{12}$$

where c_r is the condensation constant hardwired to 100 s^{-1}, ρ_l is the density of liquid water, and s is the local phase saturation. p_{sat} indicates the water saturation pressure, which is temperature-dependent.

For GDLs and CLs,

$$\frac{\partial(\varepsilon\rho_l s)}{\partial t} + \nabla\left[\rho_l\frac{Ks^3}{\mu_l}\frac{dp_c}{ds}\nabla s\right] = r_w \tag{13}$$

$$p_c = \frac{\sigma\cos\theta_c}{(K/\epsilon)^{0.5}}(1.417(1-s) - 2.12(1-s)^2 + 1.263(1-s)^3)\cdots\cdots\theta_c < 90^\circ \tag{14}$$

$$p_c = \frac{\sigma\cos\theta_c}{(K/\epsilon)^{0.5}}(1.417s - 2.12s^2 + 1.263s^3)\cdots\cdots\theta_c > 90^\circ \tag{15}$$

https://doi.org/10.1021/acsomega.3c08298
ACS Omega 2024, 9, 1683−1694

where p_c is the capillary pressure, σ is the surface tension, and θ_c is the contact angle.

2.4. Assumptions and Boundary Conditions. The following assumptions are made in the model calculations:

1. All gas is incompressible, and the cell operates under steady conditions.
2. The gas flow in the flow channel is laminar.
3. The GDL, CL, and proton exchange membrane are all isotropic, and the membrane does not allow gas to pass through.
4. The contact resistances between different layers are neglected.

In this study, the boundary conditions are established based on the assumptions and the conservation equations. The water saturation is zero at the inlet of channels. It is assumed that hydrogen and oxygen flow in the same direction. Some boundary condition parameters are also listed in Table 2. Additionally, the anode and cathode inlets are subjected to velocity boundary conditions, and the inlet velocities of hydrogen and oxygen are determined using the following formula:

$$v_{an,in} \geq \frac{1}{2F}\frac{\xi_{H_2}}{r_{H_2}}\frac{M_{H_2}}{RT_{init}}\frac{1}{p_{ref}}I_m L \quad (16)$$

$$v_{ca,in} \geq \frac{1}{4F}\frac{\xi_{O_2}}{r_{O_2}}\frac{M_{O_2}}{RT_{init}}\frac{1}{p_{ref}}I_m L \quad (17)$$

where ξ_{H_2} and ξ_{O_2} are the reactant stoichiometric flow ratio of the anode and cathode, respectively. I_m is the reference density.

2.5. Grid Independence and Validation. This study investigates the influence of the number of meshes on the simulation results to ensure independence. Meshing is done by using tetrahedral and hexahedral methods. The GDL, CL, and membrane are encrypted to improve gas diffusion and calculation accuracy. Case A is used to test grid independence. As shown in Figure 3, it can be obviously seen that the polarization curves are consistent when the grid numbers are 154563, 386210, 608674, and 1006523, respectively. Results show that the calculation error is within 1% when the number of grids exceeds 386210.

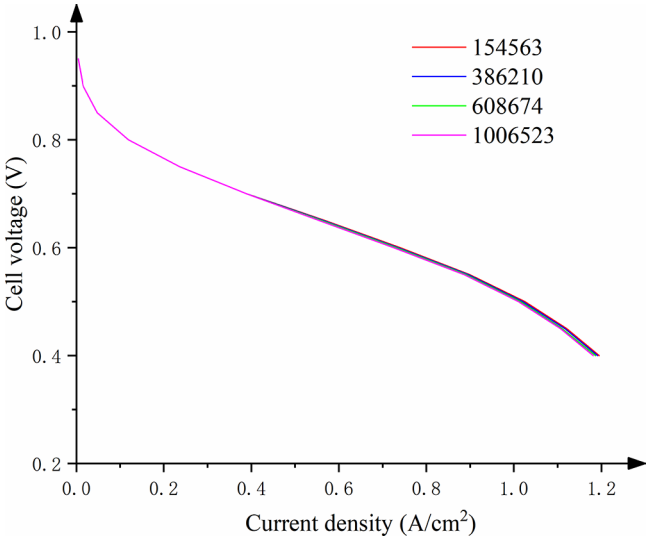

Figure 3. Results of the grid independent test.

To validate our model, we compared the simulation data obtained from the reference model with the experimental study conducted by Wang et al.,[38] as shown in Figure 4. The results

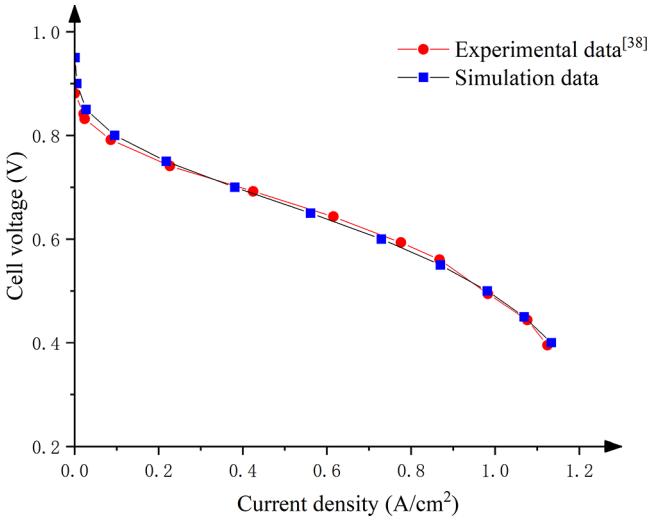

Figure 4. Model validation of the simulation results by comparison with polarization curves obtained from the experimental data.

reveal that the corresponding voltages at 0.2, 0.4, 0.6, 0.8, and 1 A/cm^2 are 0.76 0.69, 0.64, 0.58, and 0.48 V, respectively. The errors associated with these values are 1.33, 0.43, 1.39, 1.54, and 0.52%, respectively. These voltage errors with the experiments are all within 2%, indicating that the numerical simulation results are in good agreement with the experiments.

3. EVALUATION

3.1. TOPSIS Modeling. TOPSIS is a highly effective and widely used method for multicriteria decision-making. It utilizes standardized data processing to eliminate the influence of different scales and provides a more intuitive and scientific representation of the original information. The TOSPIS method does not require a specific distribution or number of study samples, making it more applicable in various evaluation fields.[39] The specific steps of TOPSIS are shown in the Supporting Information.

A comprehensive evaluation model of PEMFC was established using the TOPSIS method, as depicted in Figure 5. The model comprises two layers and encompasses five subperformances categories and eleven indicators. These subperformances provide an assessment of the overall performance of proton exchange membrane fuel cells (PEMFCs) based on energy and economic analyses. Further details regarding the subperformance and indicators are analyzed below.

3.2. Power Analysis. The output capability of PEMFCs is commonly assessed through their maximum power density. A higher maximum power density results in a higher output power for the PEMFC. PEMFCs with blockages can enhance their output performance, but this also leads to an increase in the pressure drop and power required for pumping. Therefore, when the energy utilization capability of a PEMFC is evaluated, both maximum power density and the pressure drop should be considered. The pressure drop is taken as a negative indicator.

https://doi.org/10.1021/acsomega.3c08298
ACS Omega 2024, 9, 1683−1694

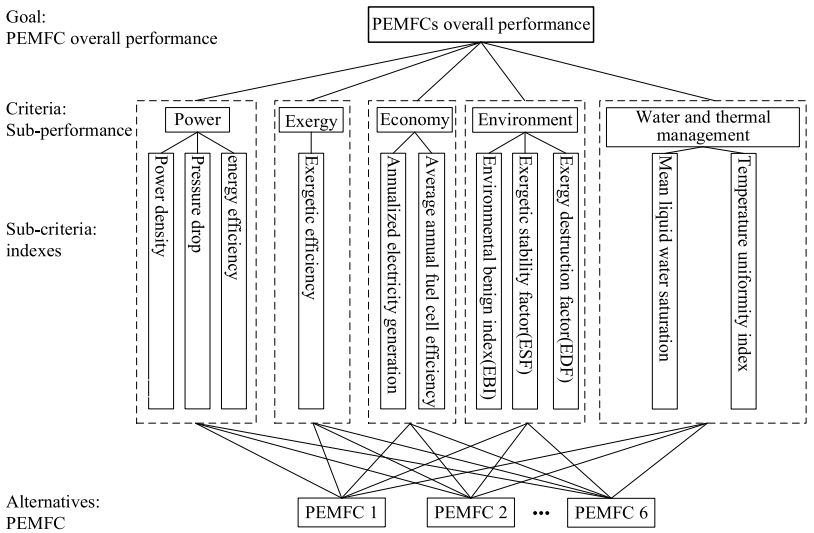

Figure 5. TOPSIS comprehensive evaluation model.

Typically, the maximum power density needs to be increased, while the reduction of pressure drop is favorable.

3.3. Exergy Analysis. Exergy refers to the effective or available energy of a system in a specific state. It also represents the maximum useful work that the system can release upon transitioning from that state to the ambient state. In the PEMFC, exergy analysis can provide valuable information regarding the useful work that can be obtained from the second law of thermodynamics. This analysis can be used to optimize the efficiency of heat dissipation, making exergetic efficiency a crucial indicator for evaluating the quality of energy utilization in PEMFC.

3.4. Economic Analysis. The economics of PEMFC involve assessing energy efficiency and cost savings. Usually, the analysis requires consideration of capital costs, fuel costs, and maintenance operating costs. This study focuses on the PEMFC single-unit design and therefore excludes maintenance and operation costs. Capital cost refers to the cost of each component of the PEMFC, including assembly. The research primarily involves changing the shape of the PEMFC bipolar plate. Despite the different shapes of bipolar plates in the various schemes, the cost difference is negligible due to the large production quantity during the actual production process. As for fuel cost, this research only considers the change in the shape of the flow channel and thus assumes no difference exists in the fuel cost of PEMFC. Therefore, the cost analysis mainly focuses on the differences in power generation.

$$\text{Cost} = \frac{\text{ACC} + \text{AFC}}{\text{AEP}} \tag{18}$$

where ACC is the annual cost of capital, AFC is the annual fuel costs, and AEP is the annual power generation.

The annual generation rate of PEMFC is defined as follows:

$$\text{AEP} = (P_{\text{fc}} \times 8760)\frac{\text{CF}}{1000} \tag{19}$$

where P_{fc} is the power of PEMFC. CF represents the capacity factor. The capacity factor values can be considered 0.5.

The gradual increase in the PEMFC efficiency is expected to accelerate the current PEMFC technologies. The average annual efficiency (AAE) of a PEMFC during operation can be expressed as follows:

$$\text{AAE} = \frac{1}{1.482}\left[\sum_j V\left(\Xi_j\right)\tau_j\right] \tag{20}$$

where $V(\Xi_j)$ is the cell potential at any given power level, and C_{fuel} is the portion of time operating at the power level.

3.5. Environmental Analysis. Most energy production systems have pros and cons for the environment. Even though fuel cells are considered environmentally friendly, they can have negative impacts. To evaluate the environmental impact of PEMFC, an analysis based on the second law of thermodynamics is conducted. The environmental benign index (EBI), energy stability factor (ESF), and environmental destruction factor (EDF) can be used as indicators to assess the system's environmental friendliness.[33] These indicators are related to useful work, exergy, and entropy increase.

3.6. Water and Thermal Quantification Analysis. In the practical application of PEMFC, the high current density is beneficial for increasing power density and reducing cost.[40] However, it can also lead to cathode flooding owing to the increased generation of water. This study uses liquid water volume as an evaluation index for PEMFC's water management, with the average liquid water saturation (MLWS) being the evaluation parameter. The liquid water saturation for each grid is calculated based on eqs 13−15, and then, the average liquid water saturation for a region is calculated after eq 21. The higher the liquid water content, the worse the water management effect.

$$s_{\text{average}} = \frac{1}{V}\int s \cdot \mathrm{d}V \tag{21}$$

where V is the total volume of the GDL and CL.

The temperature of each part of the PEMFC membrane is inconsistent because of the electrochemical reactions. This causes thermal stress and uneven deformation, which can reduce cell life. The temperature uniformity index (TUI) is used as an indicator to evaluate the thermal performance of the PEMFC. A lower value represents greater uniformity. The calculation process for TUI is provided in the study.

$$\overline{T} = \frac{1}{n}\sum_{i=1}^{n} T_i \tag{22}$$

https://doi.org/10.1021/acsomega.3c08298
ACS Omega 2024, 9, 1683−1694

$$\sigma = \sqrt{\frac{1}{n}\sum_{i=1}^{n}(T_i - \overline{T})^2} \tag{23}$$

$$U = 1 - \frac{\sigma}{\overline{T}} \tag{24}$$

where T_i is the temperature of the membrane. It is calculated based on each grid.

4. RESULTS AND DISCUSSION

4.1. Effect of Blockage Shapes in the Channel for PEMFC. *4.1.1. Polarization Curves and Power Density.* This study evaluates the performance of PEMFC using the polarization curve as an important criterion. Figure 6 displays

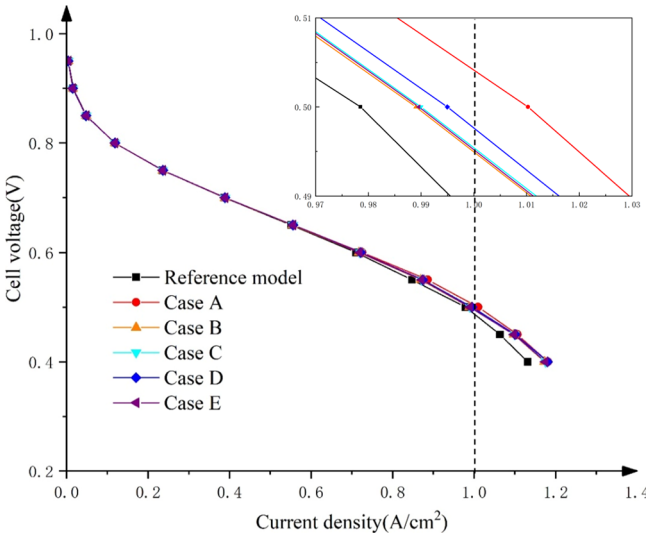

Figure 6. Polarization curves of PEMFC under different blocks shapes in the channel.

the polarization curves of PEMFCs with various blocking structures. The results indicate that the incorporation of a blockage in the flow channel has a positive effect, particularly in the high current density region. This might be attributed to the nozzle-type effect produced by the reaction gas that flows through the blockage. The blockage design enhances gas turbulence and improves the mass transfer effect inside the PEMFC. The study shows that Case A shows the best improvement of cell voltage at a certain current density. The cell voltages rank from high to low as Case A > D > C > E > B. When the current density is 1A/cm^2, the voltage of Case A is 0.504 V, which is increased by 3.42% compared to the reference model with a voltage of 0.487 V. Case B has a voltage of 0.493 V, an increase of 1.29%; Case C has a voltage of 0.494 V, an increase of 1.48%; Case D has a voltage of 0.496 V, an increase of 1.88%; and Case E has a voltage of 0.494 V, an increase of 1.33%.

The power density comparison is presented in Figure 7. It indicates that adding a blockage can increase the output power. The power increase and polarization curve follow the same trend, with the maximum power density achieved at around 0.5 V. Case A shows the most significant improvement in output power, with a maximum output power density of 0.505W/cm^2. A 3.24% increase is observed in Case A compared with the reference model's maximum output power density of 0.489W/cm^2. Case B has a maximum power density of 0.494 W/cm^2, an increase of 1.07%; Case C has a maximum power density of

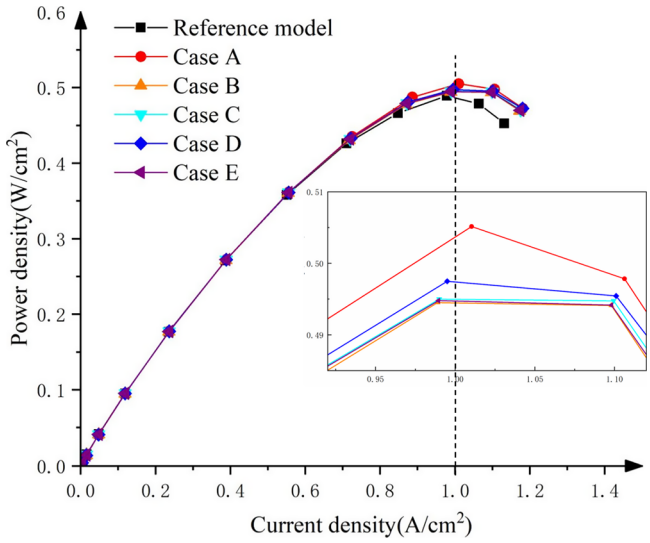

Figure 7. Power density curves of PEMFC under different block shapes in the channel.

0.495 W/cm^2, an increase of 1.17%; Case D has a maximum power density of 0.497 W/cm^2, an increase of 1.68%; Case E has a maximum power density of 0.495 W/cm^2, an increase of 1.13%.

4.1.2. Overpotential Analysis. During the electrochemical reaction process, several factors can contribute to a permanent loss of voltage output in the PEMFC, which is referred to as battery overpotential. The metal phase in the cathode CL should be lower than the average value to boost the ORR rate. Therefore, the cathode overpotential is negative.[41] Based on eq 16, the overpotential affects the electrode current density, and a higher cathode overpotential results in a greater current density.

Figure 8 displays the overpotential values for the reference model and the different models. We study the overpotential values at the midline of the cathodic GDL and CL interfaces at 0.5 V. Table 3 provides the overpotential values at the cathode GDL and CL interfaces at a distance of 25 cm from the inlet. The overpotential is visually displayed by using a positive number. Table 3 provides evidence that the PEMFC with different

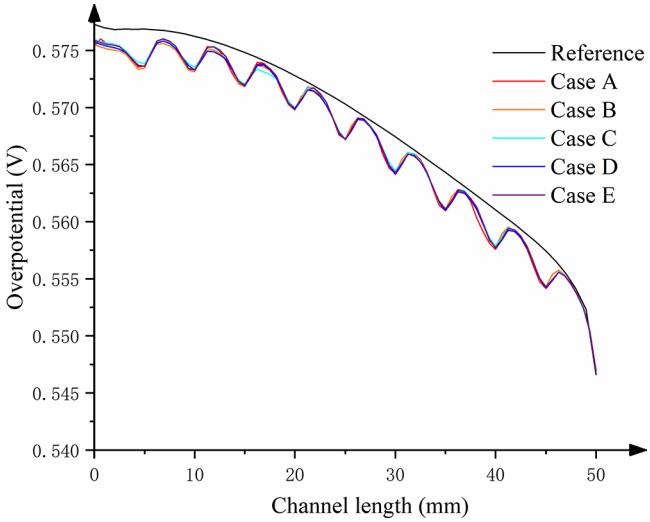

Figure 8. Overpotential of the centerline of the interface between CL and GDL at 0.5 V.

https://doi.org/10.1021/acsomega.3c08298
ACS Omega 2024, 9, 1683−1694

Table 3. Overpotential Values at the Cathode GDL and CL Interfaces

	reference	case A	case B	case C	case D	case E
overpotential (V)	0.57029	0.56723	0.56723	0.56723	0.56718	0.56721

blockages exhibits a smaller overpotential. Among the cases, Case D shows the smallest overpotential, which is 0.00311 V less than that of the reference model. The blocked PEMFC has a smaller overpotential value and a smaller voltage loss. After adding a blockage in the flow channel, the accumulation of moisture at the blockage increases the overpotential value.[42] This gives rise to the equilibrium potential. Even so, the overall overpotential is smaller than that of the reference model, indicating an improved performance after adding the blockage. Therefore, PEMFCs with different blockages have lower overpotentials and better energy performance.

4.1.3. Mass Transfer Analysis. Figure 9 shows the concentration of oxygen along the flow direction in the midline

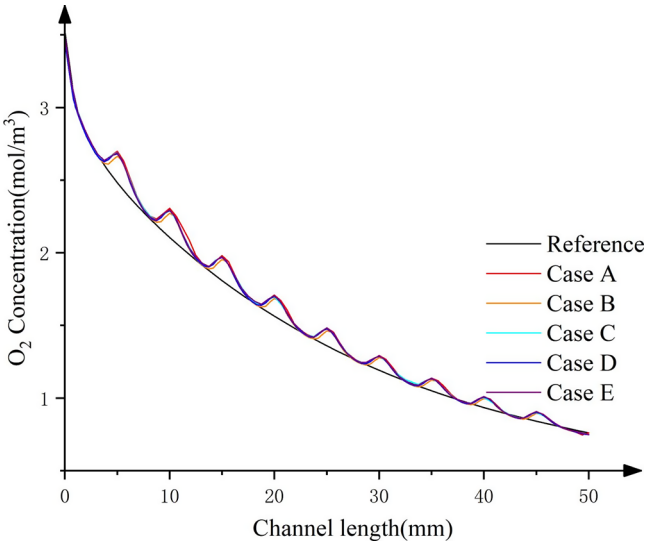

Figure 9. O_2 concentration on the centerline of the interface between CL and GDL at 0.5 V.

of the interface between GDL and CL. The addition of blockages in the flow channel affects the distribution of the reactant concentration. As the electrochemical reaction consumes oxygen, its concentration decreases gradually with the flow direction. The study found that the addition of blocking promoted the transport of oxygen. The disturbed flow by blockages leads to a higher oxygen concentration in PEMFC with different blockages than the reference model. Table 4 shows the oxygen concentration measured at the cathode GDL and CL interfaces at 25 cm from the inlet. The highest local oxygen concentration and best energy performance are observed in Case A. The order of oxygen concentration in different cases is Case A > D > C > E > B, indicating that the elliptical blockage has the strongest disturbing effect on the gas flow.

4.1.4. Flow Velocity and Pressure Drop. The concentration of reactants and fluid flow conditions play crucial roles in the electrochemical reaction. Figure 10 demonstrates the oxygen

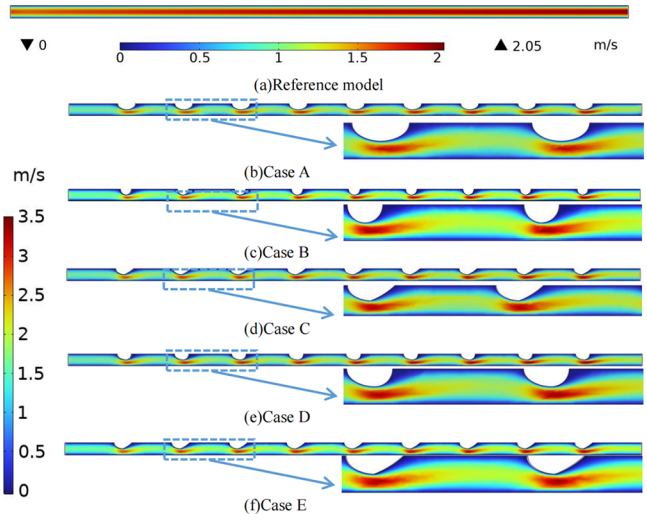

Figure 10. Velocity distribution of different cases at 0.4 V.

flow velocity in the flow channels of various cases. The blockage in the flow channel leads to a significant increase in oxygen flow velocity, with the highest velocity observed at the top of the streamlined blockage. This increase in velocity is caused by the nozzle effect. It occurs when the cross-sectional area of the reacting gas is reduced as it flows through the blockage. Table 5 demonstrates the maximum flow rate and pressure drop in the cathode flow channel at 0.4 V. Case D exhibits the highest maximum flow velocity up to 3.4522m/s, indicating that the combination of elliptical and circular streamlines results in the greatest increase in the flow rate.

The streamlined model has the advantage that it exhibits low flow resistance while increasing airflow disturbance. This contributes to the reduced friction between the fluid and the obstruction as it flows through. The cathode pressure drop of PEMFC is shown in Figure 11. As the PEMFC output voltage decreases, the resulting pressure drop tends to increase. This is because the PEMFC current density increases, generating more water in the cathode reaction. The overall pressure drop is ranked as Case A > D > C > E > B. Case A exhibits the largest pressure drop, with an improvement of 23.8371 Pa compared to the reference model. Case B has the least pressure drop. We speculate that the least blocked volume and the least resistance to flow reduce the pressure drop. Compared to 4.1.2, Case A has a larger pressure drop but a higher local oxygen concentration, while Case B has the smallest pressure drop and a lower local oxygen concentration. The pressure drop in the remaining cases also had an opposite trend to the local oxygen concentration. Therefore, the evaluation of PEMFC is less reasonable if it targets a single indicator. Moreover, the single-objective evaluation may have contradictory results when different indicators are selected. Therefore, when it comes to the

Table 4. Oxygen Concentration at the Cathode GDL and CL Interfaces

	reference	case A	case B	case C	case D	case E
concentration of O_2 (mol/m3)	1.3597	1.4843	1.4718	1.4826	1.4835	1.4811

https://doi.org/10.1021/acsomega.3c08298
ACS Omega 2024, 9, 1683−1694

Table 5. Pressure Drop and Maximum Flow Rate in the cathode Flow Channel

	reference	case A	case B	case C	case D	case E
velocity of O_2 (m/s)	2.0145	3.4005	3.4224	3.4168	3.4522	3.4425
pressure drop (Pa)	21.4388	45.27593	41.17456	42.48926	43.47833	42.40838

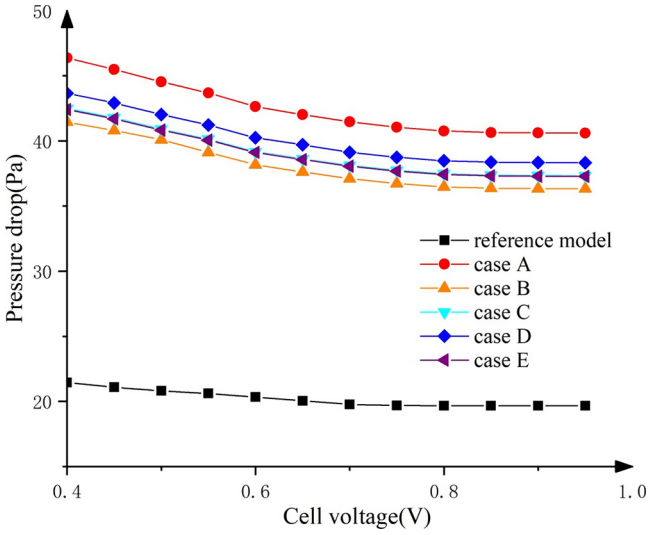

Figure 11. Pressure drop of different cases at 0.4 V.

evaluation in this study, we choose a multiobjective method to complete the comparison among various cases.

4.1.5. Water Removal. The MLWS of the cathode has been presented in Table 6. All PEMFCs with blockages showed a reduction in MLWS when compared with the reference model. Among them, Case D demonstrates the lowest MLWS with a 35.8% decrease at 0.6 V, indicating its superior capability to remove liquid water. This is caused by the enhanced purging effect of adding a blockage, thus increasing the liquid water removal capacity. This leads to an increase in the cell's capacity to remove liquid water. Additionally, the current study assumes a uniform mist flow through a short channel, which results in minimal liquid water saturation. Under such conditions, the introduction of streamlined blockages can have a positive impact on liquid water removal from the cell.

4.2. Results of TOPSIS Analysis. *4.2.1. Scores.* Table 7 displays the initial values of each index in the TOPSIS model. It can be seen that the data exhibit a small difference between the data; this is because we are studying a single cell. If the whole battery stack is studied, then it will show a large difference. Simulation results provide the values for power density and pressure drop, while the remaining indicators require calculation using eqs 19−24. The negative indicators include pressure drop, ESF, MLWS, and TUI, whereas the positive indicators comprise the rest.

Among the reference model and the conventional PEMFC, PEMFCs with blockages exhibit superior performance in output-related indicators, such as power density, energy efficiency, and exergetic efficiency. However, they perform poorly in pressure drop and EDF. This suggests that while PEMFCs with blockages enhance output performance, they also increase system entropy and lead to confusion. Among the PEMFCs with blockages, Case A outperforms the others in terms of its highest power density, efficiency, and exergy efficiency. Compared to the reference model, Case A is 3.24% more energy-efficient and 3.25% more exergetic-efficient. However, it also exhibits the largest pressure drop and EDF, indicating a significant irreversible energy loss. Compared to the reference model, Case A has a 100.6% higher pressure drop and 3.82% higher EDF. While the reference model may have the lowest energy performance, it compensates by having the least pressure drop loss and the highest environmentally friendly performance.

It is important to note that the subperformance of AAE is the same across all cases, as the voltage of the PEMFC running at maximum power is 0.5 V. While this subperformance value cannot differentiate between comparison cases, ignoring it would result in an imperfect comprehensive evaluation.

4.2.2. Comprehensive Evaluation. The TOPSIS evaluation method is used to calculate the distances between each solution and the positive and negative ideal solutions. The relative proximity is then computed for ranking purposes. The calculation process is obtained through SPSSAU, and the comprehensive scoring results are displayed in Table 8. The overall performance rankings, from the best to worst, are Case A, Case D, Case B, Case C, Reference model, and Case E. After a thorough evaluation, it is determined that Case A demonstrated the best overall performance, being the closest to the positive ideal solution and furthest from the negative ideal solution. Case D is deemed the second best.

The subperformance of the PEMFCs is plotted together for visualization. All data have been converted to positive numbers, and the range is 50−100. The subperformance based on the radar plot is shown in Figure 12. The chart shows a large gap between the index values of the reference model. The pressure drop, ESF, and EDF are the best, while the other indexes are the worst among all cases. The pressure drop and entropy increase of a reference model are better. This is because of less energy loss in the flow channel without a blockage. Case A has the best subperformance indicators such as energy density and energy efficiency. Case A has the best overall rating scores, and therefore, it is the best-optimized case. The trend of each indicator of Case D is similar to that of Case A but lower than that of Case A. The subperformance of Case B is relatively uniform, and it has the best performance on TUI. Each subperformance index of Case C and Case E is very close, mainly for their highly similar shapes.

Table 6. Mean Liquid Water Saturation of the Cathode at 0.6 V

	reference	case A	case B	case C	case D	case E
0.95 V	1.072×10^{-6}	1.064×10^{-6}	1.069×10^{-6}	1.063×10^{-6}	1.060×10^{-6}	1.064×10^{-6}
0.80 V	6.766×10^{-6}	5.731×10^{-6}	5.735×10^{-6}	5.729×10^{-6}	5.724×10^{-6}	5.731×10^{-6}
0.60 V	1.562×10^{-5}	1.008×10^{-5}	1.010×10^{-5}	1.007×10^{-5}	1.003×10^{-5}	1.008×10^{-5}
0.40 V	8.024×10^{-5}	3.442×10^{-5}	3.452×10^{-5}	3.429×10^{-5}	3.420×10^{-5}	3.440×10^{-5}

https://doi.org/10.1021/acsomega.3c08298
ACS Omega 2024, 9, 1683−1694

Table 7. Original Data of PEMFCs

		reference	case A	case B	case C	case D	case E
power	power density (W/cm^2)	0.4893	0.5051	0.4945	0.4950	0.4975	0.4948
	pressure drop (Pa)	20.81	43.83	39.63	40.90	41.88	40.83
	energy efficiency	0.2804	0.2895	0.2834	0.2837	0.2851	0.2836
exergy	exergetic efficiency	0.1568	0.1619	0.1585	0.1586	0.1594	0.1586
economy	annualized electricity generation (kWh)	2.143	2.212	2.167	2.168	2.179	2.167
	average annual fuel cell efficiency	0.3374	0.3374	0.3374	0.3374	0.3374	0.3374
environment	environmental benign index (EBI)	0.3344	0.3470	0.3383	0.3387	0.3408	0.3386
	exergetic stability factor (ESF)	0.0964	0.0960	0.0940	0.0942	0.0945	0.0941
	exergy destruction factor (EDF)	0.6548	0.6798	0.6823	0.6815	0.6820	0.6822
water and thermal management	MLWS	1.562×10^{-5}	1.008×10^{-5}	1.010×10^{-5}	1.007×10^{-5}	1.003×10^{-5}	1.008×10^{-5}
	TUI	0.9860	0.9838	0.9825	0.9838	0.9836	0.9838

Table 8. Results of TOPSIS Analysis

	positive ideal solution distance	negative ideal solution distance	relative proximity	ranking
reference model	2.646	1.732	0.396	5
case A	1.416	2.654	0.652	1
case B	2.217	1.598	0.419	3
case C	2.178	1.431	0.397	4
case D	1.926	1.690	0.467	2
case E	2.231	1.409	0.387	6

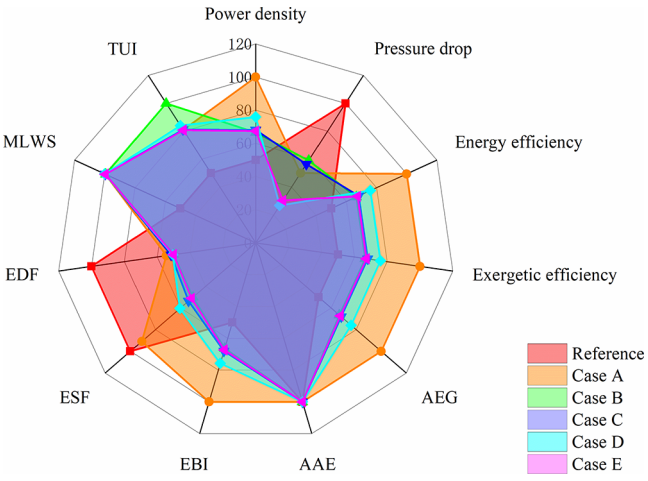

Figure 12. Radar chart-based subperformance evaluation.

5. CONCLUSIONS AND DISCUSSION

This study focuses on designing five PEMFCs with different streamlined blockages and analyzing the effects of these blockages on the PEMFC's output performance. To comprehensively evaluate the overall performance, the study utilizes TOPSIS. The conclusions drawn from the study are as follows:

1. The introduction of five different blockages in PEMFC channels has been found to enhance the output performance. Among the various blockages, elliptical-shaped ones have shown the most significant improvement, resulting in a 3.42% increase in electrochemical conversion efficiency and a 3.24% boost in maximum power density. The inclusion of blockages has not only improved the transmission quality within the channel but also increased the absolute value of the overpotential, leading to a faster reaction rate.

2. The study shows that PEMFC with blockage has a better water and thermal management performance. The blockage helps remove liquid water by increasing the flow rate and reducing the average liquid water saturation. Among all of the cases studied, Case D has the best liquid water removal with a 35.8% average saturation reduction compared to the reference model. This indicates that adding blockages has a positive effect on PEMFC water management. Additionally, the increased flow rate leads to more uniform heat transfer and lower TUI values in the PEMFC, demonstrating a better thermal management performance. Therefore, blockages can ensure a more uniform temperature distribution along the PEMFC membrane and enhance its thermal management capabilities.

3. The analysis of the indexes of PEMFC reveals that the index with blockage exhibits improved performance and higher entropy increases. However, this also suggests that the PEMFC with blockage becomes less eco-friendly. It is noteworthy that the cost of enhancing performance is higher than energy loss.

4. In this study, the TOPSIS method is used to evaluate the variability of PEMFC's overall performance, economy, and other indicators. The results show that adding blockages to the flow channel can significantly enhance the overall performance of PEMFCs. Based on the comprehensive scoring results, Case A is identified as the most optimal configuration. Furthermore, the overall performance of the four cases proposed in this study (cases A-D) is found to be better than that of the conventional PEMFC.

5. The study reveals that PEMFC designs can result in both positive and negative changes. For example, Case A leads to improved performance but also results in an elevated pressure drop and entropy increase. It is important to note that different cases show varying levels of improvement in subperformance changes within the PEMFC. Therefore, combining different PEMFC design cases to enhance subperformance generally is a key research focus.

https://doi.org/10.1021/acsomega.3c08298
ACS Omega 2024, 9, 1683−1694

■ ASSOCIATED CONTENT

Supporting Information

The Supporting Information is available free of charge at https://pubs.acs.org/doi/10.1021/acsomega.3c08298.

Specific steps of TOPSIS (PDF)

■ AUTHOR INFORMATION

Corresponding Authors

Fangzhou Wang − *School of New Energy, Harbin Institute of Technology at Weihai, Weihai 264209, P. R. China;* orcid.org/0000-0001-7355-3376; Email: wangfz@hit.edu.cn

Jianyu Tan − *School of New Energy, Harbin Institute of Technology at Weihai, Weihai 264209, P. R. China;* orcid.org/0000-0002-2442-6837; Email: tanjianyu@hitwh.edu.cn

Authors

Dong Jiang − *School of New Energy, Harbin Institute of Technology at Weihai, Weihai 264209, P. R. China*

Xianglin Li − *Department of Mechanical Engineering and Materials Science, Washington University in St. Louis, St. Louis, Missouri 63130, United States;* orcid.org/0000-0002-0193-9410

Chenxia Wang − *School of New Energy, Harbin Institute of Technology at Weihai, Weihai 264209, P. R. China*

Complete contact information is available at: https://pubs.acs.org/10.1021/acsomega.3c08298

Notes

The authors declare no competing financial interest.

■ ACKNOWLEDGMENTS

F.W., D.J., J.T., and C.W. would like to thank the support of Key R&D Program of Shandong Province, China (2022ZLGX04, 2023SFGC0101).

■ REFERENCES

(1) Liu, C; Liu, L Optimizing battery design for fast charge through a genetic algorithm based multi-objective optimization framework. *ECS transactions* **2017**, *77* (11), 257.

(2) Liu, C; Liu, L Optimal design of Li-ion batteries through multi-physics modeling and multi-objective optimization. *Journal of The Electrochemical Society* **2017**, *164* (11), E3254.

(3) Hosseinpour, J; Chitsaz, A; Liu, L; et al. Simulation of eco-friendly and affordable energy production via solid oxide fuel cell integrated with biomass gasification plant using various gasification agents. *Renewable Energy* **2020**, *145*, 757−771.

(4) Guo, Y; Pan, F; Chen, W; et al. The controllable design of catalyst inks to enhance PEMFC performance: A review. *Electrochemical Energy Reviews* **2021**, *4*, 67−100.

(5) Daud, W R W; Rosli, R E; Majlan, E H; et al. PEM fuel cell system control: A review. *Renewable Energy* **2017**, *113*, 620−638.

(6) Seyam, S; Dincer, I; Agelin-Chaab, M Investigation of potential fuels for hybrid molten carbonate fuel cell-based aircraft propulsion systems. *Energy & Fuels* **2021**, *35* (12), 10156−10168.

(7) Li, X; Faghri, A; Xu, C Structural optimization of the direct methanol fuel cell passively fed with a high-concentration methanol solution. *Journal of Power Sources* **2010**, *195* (24), 8202−8208.

(8) Liu, L; Kim, G Y; Hillier, A C; et al. Microstructural and electrochemical impedance study of nickel−Ce0. 9Gd0. 1O1. 95 anodes for solid oxide fuel cells fabricated by ultrasonic spray pyrolysis. *Journal of Power Sources* **2011**, *196* (6), 3026−3032.

(9) Sahebdelfar, S.; Ravanchi, M. T. Carbon monoxide clean-up of the reformate gas for PEM fuel cell applications: A conceptual review. *Int. J. Hydrogen Energy* **2022**, *48*, 24709 DOI: 10.1016/j.ijhydene.2022.08.258.

(10) Chen, Y; Liu, Y; Xu, Y; et al. Modeling and Simulation of Membrane Electrode Material Structure for Proton Exchange Membrane Fuel Cells. *Coatings* **2022**, *12* (8), 1145.

(11) Lu, J B; Wei, G H; Zhu, F J; et al. Pressure effect on the PEMFC performance. *Fuel Cells* **2019**, *19* (3), 211−220.

(12) Yang, Y; Jia, H; Liu, Z; et al. Overall and local effects of operating parameters on water management and performance of open-cathode PEM fuel cells. *Applied Energy* **2022**, *315*, No. 118978.

(13) Chen, Q; Zhang, G; Zhang, X; et al. Thermal management of polymer electrolyte membrane fuel cells: A review of cooling methods, material properties, and durability. *Applied Energy* **2021**, *286*, No. 116496.

(14) Feng, S; Kondo, S; Kikuchi, T; et al. Development of a heat-treated polymer−polymer type charge-transfer blend membrane for application in polymer electrolyte fuel cells. *ACS Applied Energy Materials* **2019**, *2* (12), 8715−8723.

(15) Singh, R; Oberoi, A S; Singh, T Factors influencing the performance of PEM fuel cells: A review on performance parameters, water management, and cooling techniques. *International Journal of Energy Research* **2022**, *46* (4), 3810−3842.

(16) Tang, X; Zhang, Y; Xu, S Temperature sensitivity characteristics of PEM fuel cell and output performance improvement based on optimal active temperature control. *Int. J. Heat Mass Transfer* **2023**, *206*, No. 123966.

(17) Kandlikar, S G; Garofalo, M L; Lu, Z Water management in a pemfc: water transport mechanism and material degradation in gas diffusion layers. *Fuel Cells* **2011**, *11* (6), 814−823.

(18) Yu, Y; Chen, S; Wei, H Numerical study on the effect of microporous layer crack changes on water management in gas diffusion layer of proton exchange membrane fuel cell. *Int. J. Heat Mass Transfer* **2023**, *212*, No. 124275.

(19) Ijaodola, O S; El-Hassan, Z; Ogungbemi, E; et al. Energy efficiency improvements by investigating the water flooding management on proton exchange membrane fuel cell (PEMFC). *Energy* **2019**, *179*, 246−267.

(20) Harilal; Shukla, A.; Ghosh, P.C.; et al. Pyridine-bridged polybenzimidazole for use in high-temperature PEM fuel cells. *ACS Appl. Energy Mater.* **2021**, *4* (2), 1644−1656.

(21) Zhao, Q.; Guo, H.; Ye, F.; et al. State of the art of flow field plates of proton exchange membrane fuel cells. *CIESC J.* **2020**, *71* (5), 1943−1963.

(22) Li, S.; Yuan, J.; Andersson, M.; et al. Wavy surface cathode gas flow channel effects on transport processes in a proton exchange membrane fuel cell. *J. Electrochem. Energy Convers. Storage* **2017**, *14* (3), No. 031007, DOI: 10.1115/1.4036810.

(23) Perng, S W; Wu, H W A three-dimensional numerical investigation of trapezoid baffles effect on non-isothermal reactant transport and cell net power in a PEMFC. *Applied Energy* **2015**, *143*, 81−95.

(24) Shen, J; Tu, Z; Chan, S H Enhancement of mass transfer in a proton exchange membrane fuel cell with blockage in the flow channel. *Applied Thermal Engineering* **2019**, *149*, 1408−1418.

(25) Zhang, S; Qu, Z; Xu, H; et al. A numerical study on the performance of PEMFC with wedge-shaped fins in the cathode channel. *Int. J. Hydrogen Energy* **2021**, *46* (54), 27700−27708.

(26) Li, N; Wang, W; Xu, R; et al. Design of a novel nautilus bionic flow field for proton exchange membrane fuel cell by analyzing performance. *Int. J. Heat Mass Transfer* **2023**, *200*, No. 123517.

(27) Gao, W; Li, Q; Sun, K; et al. Mass transfer and water management in proton exchange membrane fuel cells with a composite foam-rib flow field. *Int. J. Heat Mass Transfer* **2023**, *216*, No. 124595.

(28) Xia, L; Yu, Z; Xu, G; et al. Design and optimization of a novel composite bionic flow field structure using three-dimensional multi-phase computational fluid dynamic method for proton exchange

membrane fuel cell. *Energy Conversion and Management* **2021**, *247*, No. 114707.
(29) Li, H W; Liu, J N; Yang, Y; et al. Research on mass transport characteristics and net power performance under different flow channel streamlined imitated water-drop block arrangements for proton exchange membrane fuel cell. *Energy* **2022**, *251*, No. 123983.
(30) Guo, H; Chen, H; Ye, F; et al. Baffle shape effects on mass transfer and power loss of proton exchange membrane fuel cells with different baffled flow channels. *International Journal of Energy Research* **2019**, *43* (7), 2737−2755.
(31) Barbir, F; Gomez, T Efficiency and economics of proton exchange membrane (PEM) fuel cells. *Int. J. Hydrogen Energy* **1997**, *22*, 1027−1037.
(32) Taner, T. Energy and exergy analysis of PEM fuel cell: a case study of modeling and simulations. *Energy* **2018**, *143*, 284−294.
(33) Bing, M.; Pouya, B.; Davood, T.; et al. Energy, exergy, environmental and economic analyzes (4E) and multi-objective optimization of a PEM fuel cell equipped with coolant channels. *Renew. Sustainable Energy Rev.* **2022**, *157*, No. 112021.
(34) Saaty, T. L. *The analytic hierarchy process: planning, priority setting, resource allocation*; McGraw-Hill: New York, 1980.
(35) Tzeng, G. H.; Huang, J. J.; Tzeng, G. H.; Huang, J. J. *Multiple attribute decision making: methods and applications[M]*; CRC Press, 2011.
(36) Hou, Y; Wang, B; Ouyang, G; et al. An Analytic Hierarchy Process to evaluate PEM fuel cell engine performance. *Int. J. Hydrogen Energy* **2011**, *36* (11), 6780−6787.
(37) Shanian, A; Savadogo, O TOPSIS multiple-criteria decision support analysis for material selection of metallic bipolar plates for polymer electrolyte fuel cell. *Journal of Power Sources* **2006**, *159* (2), 1095−1104.
(38) Wang, L; Husar, A; Zhou, T; et al. A parametric study of PEM fuel cell performances. *International journal of hydrogen energy* **2003**, *28* (11), 1263−1272.
(39) Papathanasiou, J.; Ploskas, N.; Papathanasiou, J.; Ploskas, N.; Papathanasiou, J.; Ploskas, N.; Papathanasiou, J. et al. Topsis. In *Multiple Criteria Decision Aid: Methods, Examples and Python Implementations*; Springer, 2018, pp. 1−30.
(40) Kotaka, T; Tabuchi, Y; Mukherjee, P P Microstructural analysis of mass transport phenomena in gas diffusion media for high current density operation in PEM fuel cells. *Journal of Power Sources* **2015**, *280*, 231−239.
(41) Min, C H; He, Y L; Liu, X L; et al. Parameter sensitivity examination and discussion of PEM fuel cell simulation model validation: Part II: Results of sensitivity analysis and validation of the model. *Journal of power sources* **2006**, *160* (1), 374−385.
(42) Fan, L; Niu, Z; Zhang, G; et al. Optimization design of the cathode flow channel for proton exchange membrane fuel cells. *Energy conversion and management* **2018**, *171*, 1813−1821.

https://doi.org/10.1021/acsomega.3c08298
ACS Omega 2024, 9, 1683−1694